A theoretical analysis on Rayleigh–Taylor and Richtmyer–Meshkov mixing

2005 J. Phys. A: Math. Gen. 38 6613

(http://iopscience.iop.org/0305-4470/38/29/015)

INSTITUTE OF PHYSICS PUBLISHING JOURNAL OF PHYSICS A: MATHEMATICAL AND GENERAL

J. Phys. A: Math. Gen. **38** (2005) 6613–6622 doi:10.1088/0305-4470/38/29/015

A theoretical analysis on Rayleigh–Taylor and Richtmyer–Meshkov mixing

Yigang Cao and W K Chow

Department of Building Services Engineering, The Hong Kong Polytechnic University, Hong Kong, People's Republic of China

E-mail: beygcao@polyu.edu.hk

Received 2 December 2004, in final form 10 June 2005
Published 6 July 2005
Online at stacks.iop.org/JPhysA/38/6613

Abstract

A general buoyancy–drag model was recently proposed for describing all evolving stages of Rayleigh–Taylor (RT) and Richtmyer–Meshkov (RM) instabilities (Srebro *et al* 2003 *Laser Part. Beams* **21** 347). We modify the model and then analyse the dynamical growth of RT and RM mixing zones using a spanwise homogeneous approximation, where two sides of the mixing zones are treated as distinct and homogeneously mixed fluids in the spanwise direction. The mixing zones are found to grow self-similarly when the ratio between the average amplitudes Z_i ($i = 1$: bubbles and $i = 2$: spikes) of the mixing zones and the average wavelengths λ_i characterizing perturbations remains constant, i.e., $Z_i/\lambda_i = b(A)$, where $b(A)$ is a constant for a fixed Atwood number A. For a constant acceleration g, $Z_i = \alpha_i A g t^2$, and $Z_i \propto t^{\theta_i}$ for an impulsive acceleration. With a simple form of $b(A)$: $b(A) = \frac{1}{1+A}$, α_i and θ_i deduced agree with recent LEM (linear electric motor) data over the experimental range of density ratio R. In addition, we find $\alpha_2 \sim \alpha_1 R^{D_\alpha}$ with $D_\alpha = 0.37$ and $\theta_2 \sim \theta_1 R^{D_\theta}$ with $D_\theta = 0.24$. These agree well with recent experiments. Furthermore, as $A \to 1$, $\alpha_2 \to 0.5$ and $\theta_2 \to 1$ are derived, consistent with recent theoretical predictions.

PACS numbers: 47.20.−k, 47.20.Ma

1. Introduction

The stability of hydrodynamic flows is a fundamental issue in fluid mechanics. Small disturbances in a multifluid system produce buoyancy and shear-driven instabilities at an interface between distinct fluids [1]. Rayleigh–Taylor (RT) instability is an important hydrodynamic effect that occurs at a fluid interface where the density gradient and the acceleration are oppositely directed. A related process takes place when shock waves pass through an interface. This process is often referred to as the Richtmyer–Meshkov (RM)

instability, similar to the well-known RT instability. The presence of RT and RM instabilities has been found to be of importance to a variety of natural phenomena, including the explosion of supernovae [2], magnetized plasmas [3, 4], magnetic confinement [5], solar magnetic layers [6], inertial confinement fusion (ICF) [7], the acceleration of metal plates [8], underground salt domes [9], volcanic islands [10], and so on. At early stage, the RT instability grows exponentially with time and the RM instability grows only linearly. However, both RT and RM instabilities develop into a turbulent mixing zone at late times when the amplitude of perturbation becomes comparable to its wavelength. In the mixing zone, nonlinearities reduce the growth in an asymmetric fashion [11] and there clearly appear bubbles of light fluid and spikes of heavy fluid, each penetrating into the opposite fluid [12].

Turbulent mixing by RT and RM instabilities is a common and important phenomenon in basic science and in engineering applications. A very fundamental issue is to determine the mixing growth rate [13]. The growth of RT mixing regions depends mainly on the acceleration $g(t)$ and the density ratio $R \equiv \rho_2/\rho_1$. Here $\rho_2(\rho_1)$ is the density of heavy (light) fluid. Both the bubble ($i = 1$) and the spike ($i = 2$) amplitudes (Z_i) grow self-similarly with some acceleration distance $\propto gt^2$ [14]. For a constant acceleration g, $Z_i = \alpha_i A g t^2$ [15, 16], where $A \equiv \frac{\rho_2-\rho_1}{\rho_2+\rho_1}$ is the Atwood number. Rocket rig (RR) experiments [15] with immiscible fluids obtained $\alpha_1 = 0.06$–0.07 for bubbles. Recent linear electric motor (LEM) experiments [17] with immiscible fluids derived $\alpha_1 = 0.05 \pm 0.005$ and $\alpha_2/\alpha_1 \sim R^{D_\alpha}$ with $D_\alpha = 0.34 \pm 0.05$ over a wide range of density ratio. In contrast, the impulsive nature of RM instability does not induce such a well-defined, self-similar law of fluid interpenetration. It is recognized that bubble and spike amplitudes grow differently as $Z_i \propto t^{\theta_i}$ [18]. The exponents θ_i are thought to be universal, and experiments [17] found $\theta_1 = 0.25 \pm 0.05$ and $\theta_2/\theta_1 \sim R^{D_\theta}$ with $D_\theta = 0.21 \pm 0.05$ for $R < 50$.

However, the problem of RT and RM mixing is far from being completely resolved [19]. There are many important issues such as turbulence spectrum, molecular diffusion [13, 20–24], and so forth. Even for the mixing fronts (arrays of bubbles and spikes of the mixing zone edges), there is still no unanimous description of the dynamical evolution and the growth rate modelling is a general concern [14]. We will address buoyancy–drag models of the mixing zone growth in this paper.

On the assumption that the outer and growing length scale defined by the mixing zone width dominates the dynamics and that the influence of the small length scales within the mixing zone can be ignored for the purpose of studying the bulk motion of the mixing layer, it was believed that the buoyancy–drag model [25] based on the balance between inertial, buoyancy and Newtonian drag forces [26] could give a proper description of the evolution of the mixing zone boundaries. Since then, many articles [14, 17, 18, 27–31] on buoyancy–drag models have appeared in the literatures. In these articles, a class of attempts were made to model the growth of bubbles and spikes. These attempts include the coupled bubbles and spikes model (Youngs's model) [27], bubble competition models [18, 28] and the tube model [29]. All these models have varying degrees of success in describing the observed variation of α_i and θ_i with density ratio (or Atwood number) on the LEM. But the model equations proposed by Cheng *et al* [30] describe well the available experiments by assuming α_1 is known experimentally. Dimonte recently suggested a spanwise homogeneous buoyancy–drag model [14] in which the two sides of a mixing zone are treated as distinct and homogeneously mixed fluids in the spanwise direction. This provides a simple and intuitive technique for determining the time-dependent, volume-averaged densities in the inertia and buoyancy terms.

Most recently, based on Layzer potential flow model at an infinite density ratio ($A = 1$) [32, 33], Shvarts and co-workers [34] put forward a general buoyancy–drag model at every A for describing all evolving stages of the RT and RM instabilities. The full spectrum of

perturbations is identified with an equivalent single-mode perturbation characterized by its wavelength λ. The buoyancy–drag equation is

$$[(C_a E(t)+1)\rho_i + (C_a + E(t))\rho_{i'}]\frac{\mathrm{d}V_i}{\mathrm{d}t} = (1-E(t))(\rho_2-\rho_1)g(t) - C_d\rho_{i'}\frac{V_i^2}{\lambda} \tag{1}$$

for bubbles ($i=1$) or spikes ($i=2$) where $i'=3-i$ and $V_i = \frac{\mathrm{d}Z_i}{\mathrm{d}t}$. The parameter $C_a = 2$ and 1 for two-dimensional (2D) and three-dimensional (3D) perturbations, respectively. The drag coefficient $C_d = 6\pi$ (2D), 2π (3D). Note that the parameters C_a and C_d are not phenomenological but are the results of the bubble competition picture and of the single-mode Layzer model [31]. Also a single wavelength λ is used in this model because of the assumption that the bubbles have the same periodicity as that of the spikes. In addition, the amplitude dependence is introduced through the parameter $E(t) = \mathrm{e}^{-C_e kZ_1}$ with $C_e = 3$ for 2D and 2 for 3D perturbations [34]. The wave-vector $k = 2\pi/\lambda$. The model describes the growth of the mixing fronts for a multimode perturbation and for a general acceleration profile. In contrast with previous buoyancy–drag models [14, 17, 18, 27–31], in which only the asymptotic, i.e., self-similar, stage of RT and RM instabilities is described, equation (1) can describe all instability stages including linear, nonlinear and asymptotic stages. In the linear stage, λ is not changed with time. With the growth of the mixing zone, the wavelength characterizing the perturbation grows. Upon entering the asymptotic stage, the mixing fronts show self-similarity and the ratio between the average amplitude and the average wavelength remains constant, i.e., $Z_1/\lambda = b(A)$, where $b(A)$ is a constant for a specified Atwood number A. In reality, as $A \to 1$, this model coincides with the Layzer model for all instability stages, and for the asymptotic stage, when kZ_1 is large and $E(t) \to 0$, it is equivalent to previous buoyancy–drag model [30] with the drag coefficient C_d substituted by $C_d b(A)$. Assuming $Z_1 = Z_2$ and $b(A) = \frac{1.6}{1+A}$, Shvarts *et al* obtained the total mixing zone width, $Z_1 + Z_2$, for constant acceleration RT instability, in agreement with experiments.

But the total mixing zone width cannot give the growing information of bubbles and spikes separately. More than that, the mixing amplitudes are in general different, due to the asymmetric behaviour, not as in [34] where $Z_1 = Z_2$ was presumed. In the present paper we modify the general buoyancy–drag model described by equation (1). The single wavelength λ is replaced by λ_i (λ_1 is for bubbles and λ_2 is for spikes). Then we analyse the dynamical growth of RT and RM mixing zones using spanwise homogeneous approximation. The two sides of a mixing zone are treated as distinct and homogeneously mixed fluids in the spanwise direction. The growth rates of bubbles and spikes obtained agree with recent LEM data over the experimental range of density ratio.

2. The model

Assuming the leading edge dynamics has little influence on the internal structure of the mixing zone, the microscopic motions within the mixing zone are expected to be highly correlated and the homogeneous flow approximation [35] may be applied. This allows the two sides of the mixing zone (bubble and spike regions) to be treated as distinct and homogeneous mixed fluids in the spanwise direction. Thus a simple piecewise linear vertical density profile [14] can be used because inertia and buoyancy are volume integrated and insensitive to profile details. The LEM experiments [17] support this point. Two regions are required because the bubble (Z_1) and spike (Z_2) amplitudes are asymmetric. Consequently, the mass conservation can be written as [14]

$$(\rho_0-\rho_1)\left(\frac{Z_2}{2}\right) - (\rho_2-\rho_0)\left(\frac{Z_1}{2}\right) = 0, \tag{2}$$

where ρ_0 is the density at the initial interface location. From equation (2) we readily obtain

$$\rho_0 = \frac{\rho_1 Z_2 + \rho_2 Z_1}{Z_2 + Z_1}. \tag{3}$$

The bubble and spike regions can be considered as different buoyant objects and we construct the buoyancy–drag equations as

$$[(C_a E(t) + 1)\rho_0 + (C_a + E(t))\rho_2]\frac{\mathrm{d}V_1}{\mathrm{d}t} = (1 - E(t))(\rho_2 - \rho_0)g(t) - C_d\rho_2\frac{V_1^2}{\lambda_1} \tag{4}$$

for bubble region (between the interface and Z_1) and

$$[(C_a E(t) + 1)\rho_0 + (C_a + E(t))\rho_1]\frac{\mathrm{d}V_2}{\mathrm{d}t} = (1 - E(t))(\rho_0 - \rho_1)g(t) - C_d\rho_1\frac{V_2^2}{\lambda_2} \tag{5}$$

for spike region (between the interface and Z_2), respectively. In general, the periodicity of bubbles is different from that of spikes. Hence we use two different wavelengths λ_1 and λ_2 for bubbles and spikes in equations (4) and (5), different from [34]. In addition, here $E(t) = \mathrm{e}^{-Ce\,k_i Z_i}$.

In the asymptotic stage, bubbles and spikes grow self-similarly and Z_i/λ_i should be a constant. We assume $Z_1/\lambda_1 = Z_2/\lambda_2 = b(A)$, where $b(A)$ is a function of the Atwood number A. For a specific A, $b(A)$ is a constant. Thus the moving equations for bubble and spike regions can be rewritten as

$$\frac{\mathrm{d}V_1}{\mathrm{d}t} = \beta_1 A g(t) - C_1\frac{V_1^2}{Z_1} \tag{6}$$

and

$$\frac{\mathrm{d}V_2}{\mathrm{d}t} = \beta_2 A g(t) - C_2\frac{V_2^2}{Z_2}, \tag{7}$$

where

$$\beta_1 = \frac{(1 - E(t))(R + 1)\chi}{(C_a E(t) + 1)(\chi + R) + (C_a + E(t))R(\chi + 1)}, \tag{8}$$

$$\beta_2 = \frac{(1 - E(t))(R + 1)}{(C_a E(t) + 1)(\chi + R) + (C_a + E(t))(\chi + 1)}, \tag{9}$$

$$C_1 = \frac{C_d b(A)R(\chi + 1)}{(C_a E(t) + 1)(\chi + R) + (C_a + E(t))R(\chi + 1)} \tag{10}$$

and

$$C_2 = \frac{C_d b(A)(\chi + 1)}{(C_a E(t) + 1)(\chi + R) + (C_a + E(t))(\chi + 1)}, \tag{11}$$

with $\chi = Z_2/Z_1$.

3. Comparison with experiments

3.1. Constant acceleration case

For a constant acceleration g, the bubbles and spikes grow self-similarly as

$$Z_1 = \alpha_1 A g t^2 \tag{12}$$

and

$$Z_2 = \alpha_2 A g t^2, \tag{13}$$

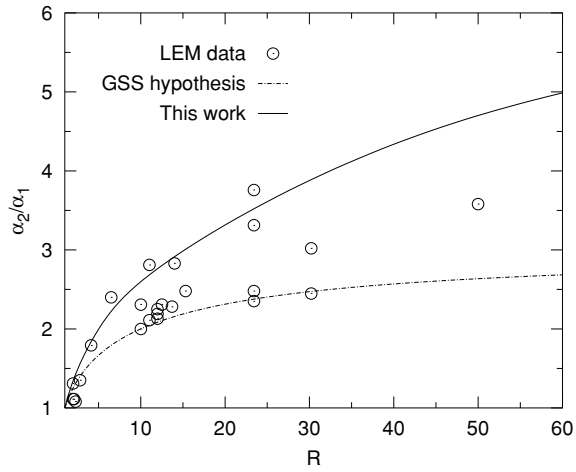

Figure 1. Density ratio dependence of α_2/α_1.

respectively. Substituting Z_i into equations (6) and (7), we get

$$\alpha_i = \frac{\beta_i}{2 + 4C_i} \tag{14}$$

for vanishing initial conditions, i.e., $V_{i0} = Z_{i0} = 0$. Therefore,

$$\frac{\alpha_2}{\alpha_1} = \chi = \frac{\beta_2}{\beta_1}\frac{2 + 4C_1}{2 + 4C_2}. \tag{15}$$

Substituting equations (8)–(11) into equation (15), we get a self-consistent equation:

$$\chi = \frac{1}{\chi}\frac{2(C_a E(t) + 1)(\chi + R) + 2(C_a + E(t))R(\chi + 1) + 4C_d b(A)R(\chi + 1)}{2(C_a E(t) + 1)(\chi + R) + 2(C_a + E(t))(\chi + 1) + 4C_d b(A)(\chi + 1)}, \tag{16}$$

which can be solved recursively.

From equation (16) it is easily derived that $\chi = 1$ as $R \to 1$ (i.e., $A \to 0$). This is because the perturbations are symmetric as $A \to 0$. With a simple form of constant $b(A)$: $b(A) = \frac{1}{1+A}$, we obtain the numerical solutions of χ for different values of density ratio R, as shown in figure 1. It should be noted that 3D values of the parameters such as C_a, C_d and C_e are utilized in our calculations in order to compare with 3D experiments. Our results are found in agreement with recent LEM data [17] over the experimental range of R. Furthermore, we fit our results to the power-law form: R^{D_α}, and find the exponent $D_\alpha = 0.37$, in good agreement with experiments [17]. For a comparison, in figure 1 we give the results obtained by the GSS hypothesis as well. GSS [36] supposed that the centre-of-mass (COM) displacement of mixing zone, L_{COM}, is much smaller than the total mixing zone width. As a consequence, the COM displacement can be treated statically, i.e., $L_{\mathrm{COM}} = 0$, compared to the mixing zone width. This hypothesis is physically plausible and depends on the self-similar growth of mixing zone. Our results support the GSS hypothesis for small density ratios ($R < 3$). But for larger density ratios, our results obviously deviate from that of the GSS hypothesis, consistent with [30].

To see clearly the growth of bubbles and spikes, we present the variation of buoyancy β_i and drag C_i coefficients with Atwood number in figures 2 and 3, respectively. For small

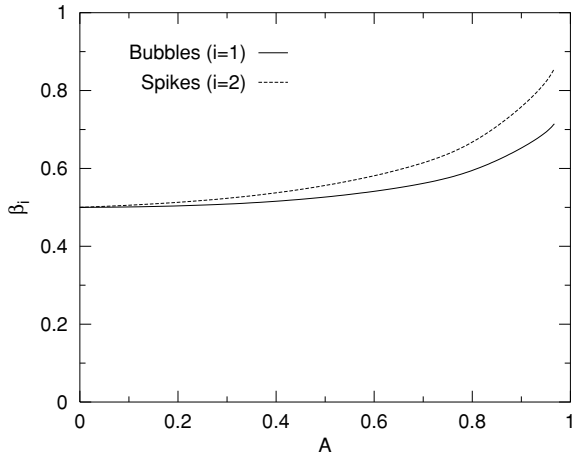

Figure 2. The variation of buoyancy coefficients β_i with Atwood number.

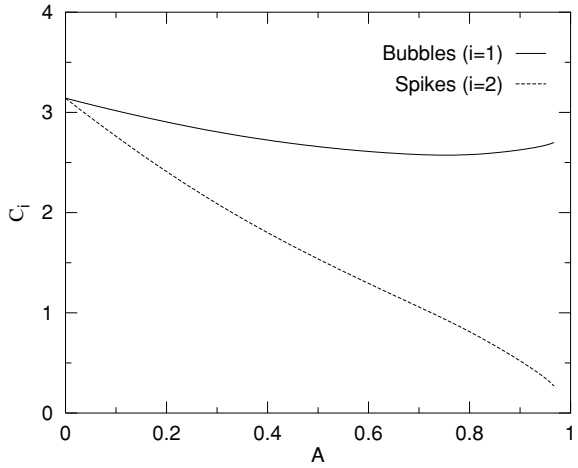

Figure 3. The variation of drag coefficients C_i with Atwood number.

values of Atwood number A, the perturbations are symmetric, i.e., $\chi \sim 1$, thus the bubble and spike factors are similar as $A \to 0$, i.e., $\beta_i \sim 0.5$, as seen in figure 2, and $C_1 = C_2$, as seen in figure 3. When $A \to 1$, $\beta_2 \to 1$ is derived. This is important because spikes require $\beta_2 = 1$ to free fall at $A = 1$. In addition, it is found in figure 3 that C_1 weakly depends on A, but C_2 declines with A because the spikes penetrate an ever more tenuous fluid. Besides, C_1 is found to be always larger than C_2 and $C_1 \gg C_2$ for $R \gg 1$, indicating that Z_1 may be the dominant length scale in the denominator of drag term for $R \gg 1$. This fact is consistent with Youngs's model [27].

Substituting the numerical β_i and C_i into equation (14), we get the growth rates α_i, as shown in figure 4, where we present the variation of α_i with Atwood number. α_1 is found insensitive to A, but a power-law increase with A is found in α_2, coincident with the results in figure 1. The obtained α_i are generally in agreement with recent LEM experiments [17]. Also, as $A \to 1$, $\alpha_2 \to 0.5$ is found. This agrees well with recent theoretical predictions [30]

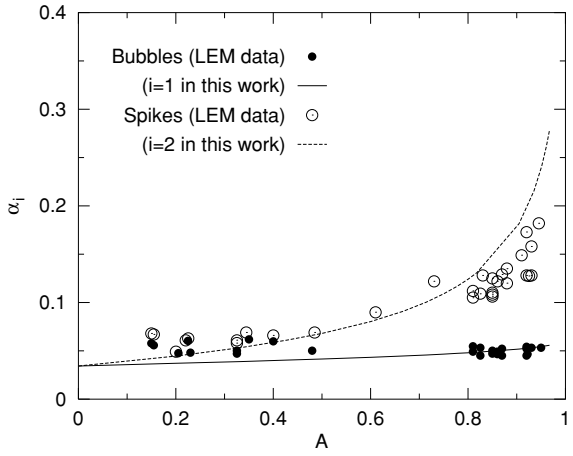

Figure 4. The variation of α_i with Atwood number.

and is reasonable in physics due to the fact that spikes fall freely when $A = 1$. But it is worth noting that α_1 is underestimated for small values of Atwood number. The underestimation may be due to the fact that the homogeneous approximation smoothes out the variance of bubbles [37].

3.2. Impulsive acceleration case

An impulsive acceleration is important because the drag term can be isolated to investigate. In RM mixing, the acceleration profile is

$$g(t) = U\delta(t), \tag{17}$$

where U is the velocity jump induced in the fluids by the impulsive acceleration. For $t > 0$, equations (4) and (5) reduce to

$$[(C_a E(t) + 1)\rho_0 + (C_a + E(t))\rho_2]\frac{\mathrm{d}V_1}{\mathrm{d}t} = -C_d\rho_2\frac{V_1^2}{\lambda_1} \tag{18}$$

for bubbles and

$$[(C_a E(t) + 1)\rho_0 + (C_a + E(t))\rho_1]\frac{\mathrm{d}V_2}{\mathrm{d}t} = -C_d\rho_1\frac{V_2^2}{\lambda_2} \tag{19}$$

for spikes, respectively. Then we get

$$\frac{\mathrm{d}V_1}{\mathrm{d}t} = -C_1\frac{V_1^2}{Z_1} \tag{20}$$

and

$$\frac{\mathrm{d}V_2}{\mathrm{d}t} = -C_2\frac{V_2^2}{Z_2}, \tag{21}$$

where C_1 and C_2 have the forms given by equations (10) and (11), respectively.

The RM bubble and spike amplitudes are supposed to have the scaling forms as

$$Z_1 = \alpha_1 t^{\theta_1} \tag{22}$$

and

$$Z_2 = \alpha_2 t^{\theta_2}. \tag{23}$$

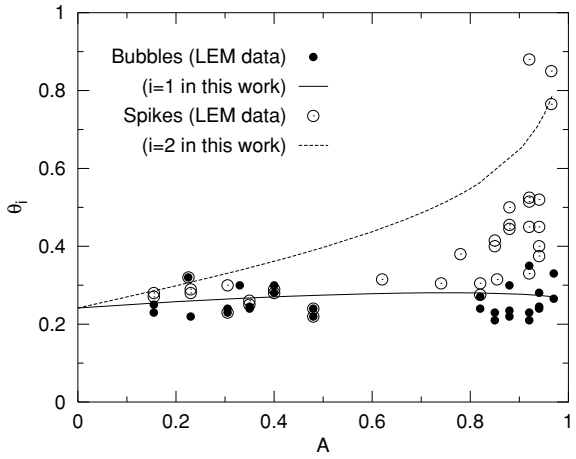

Figure 5. The variation of θ_i with Atwood number.

Here, the growth coefficients of RM mixing are assumed as that of RT mixing for simplicity. Substituting equations (22) and (23) into equations (20) and (21), respectively, we obtain the exponents

$$\theta_i = \frac{1}{1 + C_i}. \tag{24}$$

With C_i given by equations (10) and (11), we derive

$$\theta_1 = \frac{1}{1 + \frac{C_d b(A) R(\chi+1)}{(C_a E(t)+1)(\chi+R)+(C_a+E(t))R(\chi+1)}} \tag{25}$$

and

$$\theta_2 = \frac{1}{1 + \frac{C_d b(A)(\chi+1)}{(C_a E(t)+1)(\chi+R)+(C_a+E(t))(\chi+1)}}. \tag{26}$$

From equation (26), it is found that $\theta_2 \to 1$ as $A \to 1$, consistent with Cheng's prediction [30]. In addition, comparing equations (25) with (26), we find that θ_1 meets with θ_2 at $A = 0$, which is a result of symmetric perturbations as $A \to 0$. Employing the results for χ and the form of $b(A)$ in the constant acceleration case, we numerically obtain the exponents θ_i. Figure 5 shows the variation of θ_i with Atwood number. It is found that θ_1 is almost constant and in good agreement with LEM experimental data [17]. But θ_2 is found to increase with A in a power-law form. Detailed analysis tells that $\theta_2 \sim \theta_1 R^{D_\theta}$, with $D_\theta = 0.24$, in good agreement with recent LEM experiments [17], as also seen in figure 6, where the density ratio dependence of θ_2/θ_1 is presented.

4. Summary and discussion

We have modified the general buoyancy–drag model and analysed the dynamical growth of RT and RM mixing zones using spanwise homogeneous approximation. The mixing zones have been found to grow self-similarly when the ratio between the average amplitudes of mixing zones and the average wavelengths characterizing perturbation keeps constant $b(A)$ for a specific Atwood number. The mixing zone amplitudes $Z_i = \alpha_i A g t^2$ for a constant acceleration, but $Z_i \sim t^{\theta_i}$ for an impulsive acceleration. With a simple form of constant

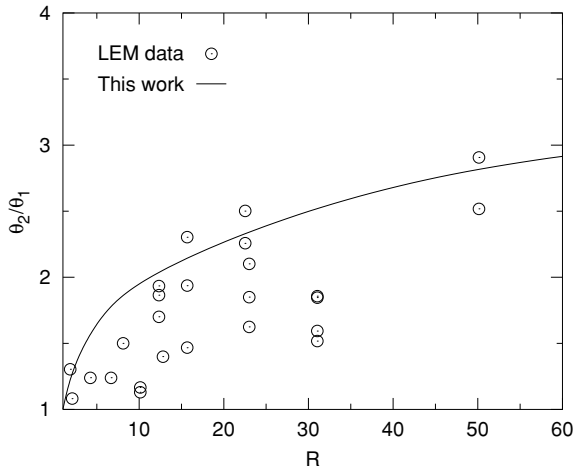

Figure 6. Density ratio dependence of θ_2/θ_1.

$b(A)$: $b(A) = \frac{1}{1+A}$, the obtained α_i and θ_i are generally in agreement with recent LEM data over the experimental range of density ratio R. Also we have found $\alpha_2 \sim \alpha_1 R^{D_\alpha}$ with $D_\alpha = 0.37$ and $\theta_2 \sim \theta_1 R^{D_\theta}$ with $D_\theta = 0.24$. These agree well with recent experiments. In particular, we have derived $\alpha_2 \to 0.5$ and $\theta_2 \to 1$ as $A \to 1$, consistent with recent theoretical predictions.

It should be emphasized that the influence of initial conditions has not been considered in our analysis. Consideration of the effects of initial conditions will improve the agreement between theoretical results and experiments [38]. Also the mixing zones include complex structures of all sizes, down to the molecular level. 'Homogeneous approximation' only provides an averaging description of the mixing zones. As pointed out in [14], the 'homogeneous approximation' describes only the self-similar phase and bypasses the initial small amplitude linear phase. A more accurate description is needed to include the initial linear terms, demixing and phase reversal [34].

Acknowledgment

The project was funded by The Hong Kong Polytechnic University under account G-YW97.

References

[1] Chandrasekhar S 1961 *Hydrodynamic and Hydromagnetic Stability* (Oxford: Oxford University Press)
[2] Arnett W D, Bahcall J N, Kirshner R P and Woosley S E 1989 *Ann. Rev. Astron. Astrophys.* **27** 629
[3] Okada S, Sato K and Sekiguchi T 1981 *Japan. J. Appl. Phys.* **20** 157
[4] Huba J D, Hassam A B and Winske D 1990 *Phys. Fluids* B **2** 1676
[5] Ferron J R, Wong A Y, Dimonte G and Leikind B J 1983 *Phys. Fluids* **26** 2227
[6] Cattaneo F and Hughes D W 1988 *J. Fluid Mech.* **196** 323
[7] Lindl J D 1998 *Inertial Confinement Fusion* (New York: Spring)
[8] Degnan J H *et al* 1995 *Phys. Rev. Lett.* **74** 98
[9] Selig F and Wermund E G 1966 *Geophysics* **31** 726
[10] Marsh B D 1979 *J. Geol.* **87** 687
[11] Kull H J 1991 *Phys. Rep.* **206** 197
[12] For a review, see Sharp D H 1984 *Physica* D **12** 3

[13] Dalziel S B, Linden P F and Youngs D L 1999 *J. Fluid Mech.* **399** 1
[14] Dimonte G 2000 *Phys. Plasmas* **7** 2255
[15] Read K I 1984 *Physica* D **12** 45
[16] Youngs D L 1989 *Physica* D **37** 270
[17] Dimonte G and Schneider M 2000 *Phys. Fluids* **12** 304
[18] Alon U, Hecht J, Ofer D and Shvarts D 1995 *Phys. Rev. Lett.* **74** 534
[19] Abarzhi S I, Glimm J and Lin A D 2003 *Phys. Fluids* **15** 2190
[20] Cook A W and Dimotakis P E 2001 *J. Fluid Mech.* **443** 69
[21] Young Y N, Tufo H, Dubey A and Rosner R 2001 *J. Fluid Mech.* **447** 377
[22] Wilson P N and Andrews M J 2002 *Phys. Fluids* **14** 938
[23] Chertkov M 2003 *Phys. Rev. Lett.* **91** 115001
[24] Ristorcelli J R and Clark T T 2004 *J. Fluid Mech.* **507** 213
[25] Lighthill M J 1986 *An Informal Introduction to Theoretical Fluid Mechanics* (Oxford: Oxford University Press)
[26] Davies R M and Taylor G I 1950 *Proc. R. Soc.* A **200** 375
[27] Hanson J C, Rosen P A, Goldsack T J, Oades K, Fieldhouse P, Cowperthwaite N, Youngs D L, Mawhinney N and Baxter A J 1990 *Laser Part. Beams* **8** 51
[28] Shvarts D, Alon U, Ofer D, McCrory R L and Verdon C P 1995 *Phys. Plasmas* **2** 2465
[29] Dimonte G and Schneider M 1996 *Phys. Rev.* E **54** 3740
[30] Cheng B, Glimm J and Sharp D H 2000 *Phys. Lett.* A **268** 366
[31] Oron D, Arazi L, Kartoon D, Rikanati A, Alon U and Shvarts D 2001 *Phys. Plasmas* **8** 2883
[32] Layzer D 1955 *Astrophys. J.* **122** 1
[33] Hecht J, Alon U and Shvarts D 1994 *Phys. Fluids* **6** 4019
[34] Srebro Y, Elbaz Y, Sadot O, Arazi L and Shvarts D 2003 *Laser Part. Beams* **21** 347
[35] Wallis G B 1969 *One-Dimensional Two-phase Flow* (New York: McGraw-Hill)
[36] Glimm J, Saltz D and Sharp D H 1998 *Phys. Rev. Lett.* **80** 712
[37] Cheng B, Glimm J and Sharp D H 2002 *Chaos* **12** 267
[38] Cheng B, Glimm J, Jin H and Sharp D 2003 *Laser Part. Beams* **21** 429